Influence of grain boundary structural evolution on pressure solution creep rates

M. P. A. van den Ende*[1,2], A. R. Niemeijer[1], and C. J. Spiers[1]

[1]High Pressure and Temperature Laboratory, Department of Earth Sciences, Utrecht University, the Netherlands

[2]Now at: Université Côte d'Azur, IRD, CNRS, Observatoire de la Côte d'Azur, Géoazur, France

Abstract

Intergranular pressure solution is a well-known rock deformation mechanism in wet regions of the upper crust, and has been widely studied, especially in the framework of compaction of granular materials, such as reservoir sandstones and fault rocks. Several analytical models exist that describe compaction creep by stress-induced mass transport, and the parameters involved are relatively well constrained by laboratory experiments. While these models are capable of predicting compaction behaviour observed at relatively high porosities, they often overestimate compaction rates at porosities below 20 % by up to several orders of magnitude. This suggests that the microphysical processes operating at low porosities are different and are not captured well by existing models. The implication is that available models cannot be extrapolated to describe compaction of sediments and fault rocks to the low porosities often reached under natural conditions. To address this problem, we propose a new, thermodynamic model that describes the decline of pressure solution rates within individual grain contacts as a result of time-averaged growth of asperities or islands and associated constriction of the grain boundary diffusion path (here termed grain boundary evolution). The resulting constitutive equations for single grain-grain contacts are then combined and solved semi-analytically. The compaction rates predicted by the model are compared with those measured in high-strain compaction experiments on wet granular halite. A significant reduction in compaction rate is predicted when grain boundary evolution is considered, which compares favourably with the experimental compaction data.

1 Introduction

Intergranular pressure solution, or dissolution-precipitation creep, is an important mechanism of time-dependent deformation of rocks under wet, upper-crustal conditions (*Lehner*, 1990; *Rutter*, 1976; *Spiers et al.*, 1990, 2004). Its relevance is recognised, in particular, in relation to the compaction of granular rock materials (*Croizé et al.*, 2010; *Gratier*, 1987; *Karner et al.*, 2003; *Spiers and Schutjens*,

*Corresponding author: martijn.vandenende@geoazur.unice.fr

1990; *Tada and Siever*, 1989), in shear deformation of dense rocks under greenschist and blueschist metamorphic conditions (*Elliott*, 1973; *Stöckhert et al.*, 1999), and in controlling the frictional behaviour and strengthening of faults (*Bos et al.*, 2000; *Blanpied et al.*, 1992; *Jefferies et al.*, 2006; *Karner et al.*, 1997; *Niemeijer and Spiers*, 2006). Crucial for the operation of pressure solution is the presence of a grain boundary solution phase in the form of an adsorbed thin film (*Robin*, 1978; *Rutter*, 1983), or of a dynamically-stable island-channel structure (*Lehner*, 1990; *Raj*, 1982; *Spiers and Schutjens*, 1990). Numerous models have been developed to describe the micro-scale processes that operate during pressure solution (e.g. *Lehner*, 1990; *Shimizu*, 1995; *Spiers et al.*, 1990), and the constitutive parameters involved have been constrained in a range of different laboratory experiments (e.g. *Dewers and Hajash*, 1995; *Gratier et al.*, 2009; *Raj*, 1982; *Rutter*, 1976; *Spiers et al.*, 1990; *van Noort et al.*, 2008). However, many experimental studies investigating densification by pressure solution consider time scales that are insufficient to reach low porosities (<15 %), being limited by the relatively slow kinetics of the process. Studies in which low porosities are achieved report compaction rates that fall orders of magnitude below values that are predicted by analytical models for pressure solution creep (*Schutjens*, 1991; *Niemeijer et al.*, 2002).

This discrepancy exposes an important shortcoming in our understanding of the micro-scale processes at play, and limits our ability to reliably extrapolate laboratory results to nature. For example, time-dependent fault zone restrengthening and fluid pressure build-up in faults have been proposed to result from densification by pressure solution creep (*Angevine et al.*, 1982; *Sleep and Blanpied*, 1992). Estimates of long-term (centennial) fault zone restrengthening accordingly require accurate descriptions of pressure solution creep over the full range of attainable fault rock porosities. As a candidate mechanism for the retardation of pressure solution at low porosities, sealing/healing of grain boundaries due to surface energy-driven mass transfer has been suggested (*Hickman and Evans*, 1991; *Van Noort et al.*, 2008; *Visser*, 1999). Crack- and grain boundary healing or sealing, driven by surface energy reduction, has similarly been suggested as a mechanism for fault rock restrengthening (*Beeler and Hickman*, 2015; *Brantley*, 1992; *Hickman and Evans*, 1992).

Here, we develop analytical expressions that describe the evolution of grain boundary structure during deformation by pressure solution, and its effect on the rate of pressure solution. To validate the model, we compare the predicted compaction rates with the laboratory data on densification of granular halite provided by *Schutjens* (1991). We find that grain boundary evolution involving increasing solid-solid contact area with time can readily explain the observed reduction in strain rate. Agreement between model and experiment is improved further if the thickness of the grain boundary zone is allowed to increase with increasing grain contact length scale, following a fractal scaling relationship.

2 Previous work on pressure solution and grain boundary healing

2.1 Pressure solution in theory and experiment

In general, pressure solution in a porous rock system where there is no long-range mass transport can be seen as a series of three consecutive processes: (1) dissolution of material at stressed grain-grain contacts, (2) diffusion of the dissolved mass out of the grain contact zone, and (3) precipitation on the pore walls. Which of these serial processes controls the overall rate of pressure solution is determined by kinetics of dissolution, diffusion, and precipitation, respectively. When it is assumed that only one process controls the kinetics of pressure solution, then for the case of either 1D or isotropic compaction, the macroscopic strain rate can be described by one of the following analytical expressions (*Pluymakers and Spiers*, 2014; *Rutter*, 1976; *Shimizu*, 1995; *Spiers and Schutjens*, 1990):

$$\dot{\varepsilon}_s = A_s \frac{I_s \Omega}{RT} \frac{\sigma_e}{d} f_s(\phi) \tag{1a}$$

$$\dot{\varepsilon}_d = A_d \frac{(DCS)\Omega}{RT} \frac{\sigma_e}{d^3} f_d(\phi) \tag{1b}$$

$$\dot{\varepsilon}_p = A_p \frac{I_p \Omega}{RT} \frac{\sigma_e}{d} f_p(\phi) \tag{1c}$$

Here, the subscripts s, d and p denote dissolution-, diffusion- and precipitation-controlled kinetics respectively, $\dot{\varepsilon}_x$ is the corresponding volumetric strain rate, A_x a geometric constant, d the mean grain size, σ_e the effective stress (applied axial stress or confining pressure minus pore fluid pressure), Ω the molar volume of the solid, R the universal gas constant, T the absolute temperature, D the effective diffusion coefficient of the ionic species dissolved in the grain boundary fluid, C the solubility of a flat, unstressed solid interface, S the (mean) thickness of fluid in the grain boundary zone, and $f_x(\phi)$ a dimensionless function of porosity (ϕ) which accounts for the evolution of contact area and pore wall area during compaction. The rate coefficients for grain boundary dissolution (I_s), precipitation (I_p) and for diffusion within the grain boundary (DCS) vary with temperature and exhibit an Arrhenius dependence on temperature, i.e. take the form:

$$I_x = I_{x,0} \exp\left(-\frac{\Delta H_x}{RT}\right) \tag{2}$$

for I_s and I_p (*Van Noort and Spiers*, 2009), and

$$(DCS) = (DCS)_0 \exp\left(-\frac{\Delta H_d}{RT}\right) \tag{3}$$

for (DCS) (e.g. *Spiers et al.*, 1990; *Spiers and Schutjens*, 1990). Here, ΔH_x is the apparent activation energy associated with each process. For highly soluble materials at room temperature, such as alkali metal salts, diffusion along the grain boundary controls the creep rate as dissolution and precipitation

are relatively fast, whereas low solubility solids often show interface reaction-controlled kinetics if the grain size is small (i.e. if the diffusion distance is short; *Niemeijer et al.*, 2002; *Spiers et al.*, 2004).

As mentioned above, the kinetics of diffusion-controlled pressure solution are governed by the combined product DCS. This parameter encompasses the structure of the grain boundary through the effective cross-section (mean fluid thickness) and the effects of any surface force interactions between the solid, the fluid, and the dissolved ionic species. Effects of grain boundary diffusion path tortuosity can be accounted for by replacing D with an effective value of D. For steady-state pressure solution, many analytical models assume a dynamically-stable island-channel grain boundary structure (*Lehner*, 1990; *Raj*, 1982; *Spiers and Schutjens*, 1990), in which contact asperities and surrounding grain boundary interfaces undergo continuous dissolution and precipitation. In this way, the grain boundary does not attain thermodynamic equilibrium, but is expected to evolve into a rough, time-statistically steady-state structure (*Lehner*, 1990), as has been observed in many laboratory experiments (*De Meer et al.*, 2002, 2005; *Renard et al.*, 2012; *Schutjens and Spiers*, 1999). However, the assumption of a steady-state grain boundary structure may be violated when the stresses on the grain-grain contacts decrease and surface energy driving forces start to play a role in controlling the energy balance within the grain boundary (*Schutjens and Spiers*, 1999; *Van Noort et al.*, 2008; *Visser*, 1999). Several experiments (e.g. *Schutjens and Spiers*, 1999) have shown that the grain boundary structure is rough and open at high effective contact stress, and much more constricted at low effective stress, indicating an evolution in grain boundary structure with decreasing contact stress. It is therefore expected that the product DCS is lower in low porosity aggregates (i.e. low contact stress) than at high porosity.

2.2 Thermodynamics of grain boundary healing and sealing

In order to further comprehend the evolution of grain contacts under stress, we will now review basic thermodynamic concepts that are prerequisites for developing a model for grain boundary structural change during compaction by pressure solution.

The chemical equilibrium at a triple junction between two grains of an isotropic solid plus a fluid phase can be described by the Young-Dupré relation (e.g. *Holness*, 1992):

$$\gamma_{ss} = 2\gamma_{sl} \cos\left(\frac{\theta_{eq}}{2}\right) \tag{4}$$

Here, γ_{sl} and γ_{ss} denote the solid-liquid and solid-solid interfacial energy, respectively, and θ_{eq} denotes the dihedral angle at equilibrium. It was shown by *Visser* and coworkers (*Visser*, 1999; *Van Noort et al.*, 2008) that when the dihedral angle θ at the contact margin deviates from the equilibrium value θ_{eq}, a thermodynamic force F (in N m^{-1}) is exerted on the contact margin, given by:

$$F = 2\gamma_{sl}\left(\cos\frac{\theta}{2} - \cos\frac{\theta_{eq}}{2}\right) = 2\gamma_{sl}\Delta\cos\frac{\theta}{2} \tag{5}$$

This force may drive lateral spreading (neck growth) or retreat (marginal dissolution or undercutting) of the solid-solid contact. A dynamically wetted island-channel structure represents a non-equilibrium, hence elevated energy state, which is thought to be maintained by local stress-induced perturbations that may overcome any surface energy reduction effects (*Lehner*, 1990; *Spiers and Schutjens*, 1990; *Visser*, 1999). However, if the stress on the grain contact is removed, or is reduced below a threshold value at which the local stress perturbations are insufficient to maintain a dynamically wetted state, the solid-liquid interfaces within a grain boundary will re-configure towards a configuration of disconnected pockets of fluids that (locally) minimises the interfacial and total energy content of the grain boundary. In the case of static growth of the asperities, this process is referred to as *grain boundary healing* (*Visser*, 1999; *Van Noort et al.*, 2008).

Following *Visser* (1999) and *Van Noort et al.* (2008), one can express the potential for lateral growth of stressed asperities within a grain-grain contact in terms of a competition between the effects of the applied stress on the elastic strain energy f_{el} and surface energy. In this treatment, the asperities are viewed as small, dynamically migrating islands with constant height and a dynamic dihedral angle of $\theta = 0$ (see Fig. 1). Then, the chemical potential $\Delta\mu_i$ (units: J m^{-3}) for lateral growth at low fluid pressures compared to the effective stress is expressed as (*Van Noort et al.*, 2008):

$$\Delta\mu_i = \frac{F}{S} - \Delta f_{el} = \frac{2\gamma_{sl}}{S}\Delta\cos\frac{\theta}{2} - \frac{(\sigma_c/\alpha)^2}{2E} \tag{6}$$

Here, Δf_{el} is the difference between the average value of f_{el} from the stressed island to the grain contact margin, σ_c denotes the mean effective normal stress on the grain contact scale (i.e. $\sigma_n - P_f$), α the relative asperity area fraction, and E the Young's modulus. If $\Delta\mu_i > 0$, lateral growth of the asperities occurs, driven by the surface energy force F (first term in the right-hand side of the equality), dominating over Δf_{el} (second term in the right-hand side). If $\Delta\mu_i < 0$, net dissolution occurs due to dominance of the stored elastic energy Δf_{el}. The criterion for static island growth, hence grain boundary healing, is then defined by the condition $\Delta\mu_i > 0$, so that the critical effective stress σ_{crit} below which healing occurs can be written in terms of the equilibrium condition:

$$\sigma_{crit} = 2\alpha\sqrt{E\frac{\gamma_{sl}}{S}\Delta\cos\frac{\theta}{2}} \tag{7}$$

For effective contact stresses lower than σ_{crit}, it is expected that the surface energy term in Eqn. (6) dominates, and that nett growth of the asperities results in healing of the grain boundary. This criterion subdivides the dynamic wetting versus grain boundary healing fields, but does not provide information regarding the rate of asperity growth in a transient state, in either stressed (pressure dissolving) or unstressed grain contacts. To gain more insight into the interplay between structural evolution of grain boundaries and compaction by pressure solution, we propose a new model below.

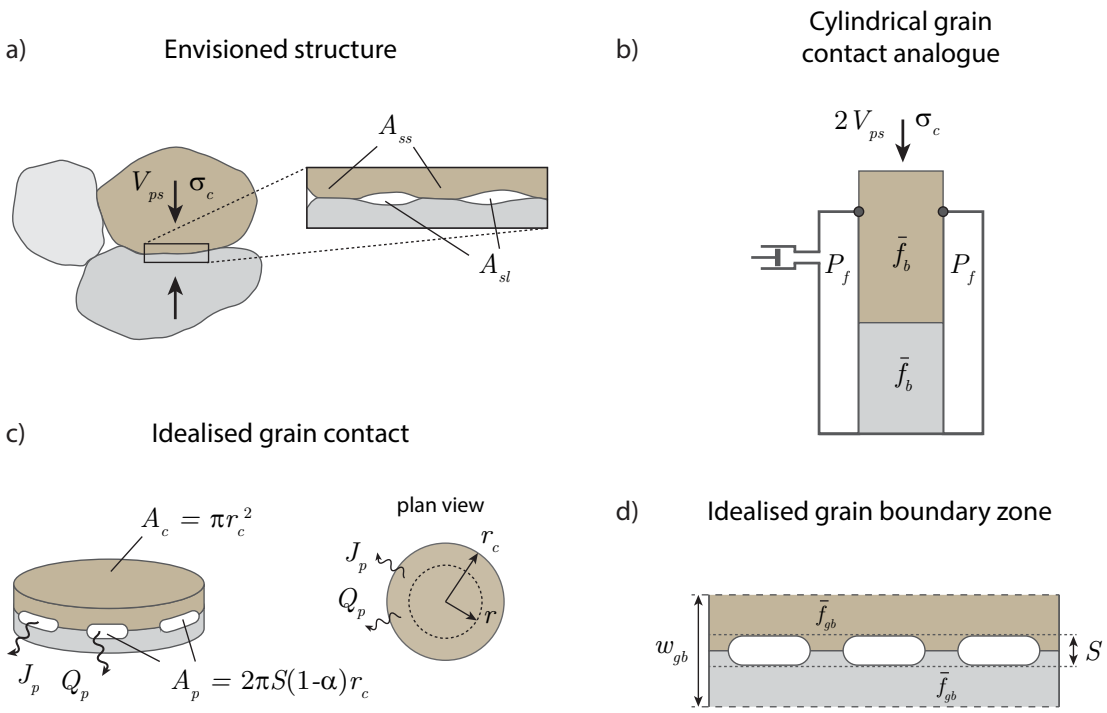

Figure 1: Synopsis of the grain geometries adopted in this work. a) During pressure solution, the envisioned grain contacts exhibit a dynamically stable island-channel structure (c.f. *Lehner*, 1990), in which the total cross-sectional area of solid-solid contact points (the islands) is A_{ss}, and the total cross-sectional area that is open to the interstitial fluid (the channels) is A_{sl}; b) In deriving the analytical constitutive relations, a cylindrical grain geometry is assumed. The solid framework is submersed in a fluid of constant pressure P_f and loaded axially with a total stress σ_c, which raises the mean free energy density of each grain to $\bar{f}_b$ and causes convergence at a rate $2V_{ps}$; c) The grain contact is envisioned as a disc-shaped region of thickness w_{gb}, cross-sectional area A_c and radius r_c. Mass is transported out of the grain contact region through the open periphery A_p; d) Within the grain boundary region, the solid has a mean free energy density $\bar{f}_{gb}$. The average height of the islands and channels is denoted by S.

3 Microphysical model for the effects of grain boundary structural change on pressure solution

3.1 Grain boundary evolution model

Following *Lehner* (1990), the grain boundary zone during pressure solution is envisioned to consist of a dynamically rough topography of contact asperities (islands) that are separated by a continuous, interconnected network of interstitial fluid (channels) – see Fig. 1. In previous studies deriving expressions for steady-state pressure solution creep, it is generally assumed that the island-channel network is a steady-state structure of which the properties, averaged over the entire grain boundary, remain constant over time (*Lehner*, 1990; *Raj*, 1982; *Spiers and Schutjens*, 1990). Similarly, we assume the average height of the grain boundary topography (S) to be time-invariant. The total

area of the grain contact A_c that is occupied by islands (i.e. solid-solid contacts) is denoted by A_{ss}. The contact area A_c increases as grain to grain convergence proceeds by pressure solution. It is convenient to define the relative island occupation ratio as $\alpha \equiv A_{ss}/A_c$. From this definition it follows that the area occupied by channels A_{sl} is $(1-\alpha)\,A_c$. During active pressure solution creep, mass is transported through the grain boundary peripheral area A_p by a diffusive flux J_p, which is defined positive when directed outward from the grain boundary into the pore space. Similarly, when the grain boundary area occupied by islands increases (i.e. when α increases), fluid is expelled out of the grain boundary, defining a positive advective flux Q_p, carrying a mean solute concentration $\bar{C}$.

Let us now consider a single disc-shaped contact between two cylindrical grains with depictions and assumptions given in Fig. 1 (specifically Fig. 1b-d). During active pressure solution with island growth, and assuming constant solid density, the mass/volume balance for the solid in the cylindrical, two-grain contact is given by:

$$\begin{aligned} 2A_cV_{ps} &= A_pJ_p + \bar{C}Q_p + \frac{\mathrm{d}\left(A_{ss}S\right)}{\mathrm{d}t} + \frac{\mathrm{d}\left(\bar{C}A_{sl}S\right)}{\mathrm{d}t} \\ &= A_pJ_p + A_cS\bar{C}\frac{\mathrm{d}\alpha}{\mathrm{d}t} + A_cS\frac{\mathrm{d}\alpha}{\mathrm{d}t} + A_c\left(1-\alpha\right)S\frac{\mathrm{d}\bar{C}}{\mathrm{d}t} - A_cS\bar{C}\frac{\mathrm{d}\alpha}{\mathrm{d}t} \\ &\approx A_pJ_p + A_cS\frac{\mathrm{d}\alpha}{\mathrm{d}t} \end{aligned} \tag{8}$$

In the first line of this equation, the different terms represent, in order: mass dissolved from the grain contact by pressure solution, the diffusive and advective mass fluxes through the grain contact periphery, respectively, the solid mass stored in the islands, and the mass stored as dissolved species in the channels (all in units $\mathrm{m^3\ s^{-1}}$). We neglect minor changes occurring in the mean solid concentration $\bar{C}$ in the grain boundary fluid. By noting that all solid volume expelled from the contact (A_pJ_p) will be precipitated on the free grain or pore walls when diffusion is rate-controlling, and that the fluid volume expelled from the grain contact must equal the increase in grain boundary island volume ($A_cS\dot{\alpha}$), the fluid volume ν^f displaced against the fluid pressure P_f must be:

$$\frac{\mathrm{d}\nu^f}{\mathrm{d}t} = A_pJ_p + A_cS\frac{\mathrm{d}\alpha}{\mathrm{d}t} = 2A_cV_{ps} \tag{9}$$

Following *Lehner* (1990, 1995), the energy/entropy balance for the two-grain system represented in Fig. 1b, neglecting contributions related to minor changes in solute concentration in the fluid phase, can be written as:

$$\dot{W} = \dot{F} + \dot{E}_s + \dot{\Delta} \tag{10}$$

where $\dot{W}$ is the mechanical work input rate, $\dot{F}$ is the rate of increase of Helmholtz energy of the solid phase, $\dot{E}_s$ accounts for the changes in surface stored energy caused by island growth/contraction, and $\dot{\Delta} \geq 0$ is the rate of dissipation due to irreversible processes (all in units of $\mathrm{J\ s^{-1}}$).

For the nett work input rate, we can write (using Eqns. (8) and (9)):

$$\dot{W} = 2\sigma_c A_c V_{ps} - P_f \frac{\mathrm{d}\nu^f}{\mathrm{d}t} = 2\left[\sigma_c - P_f\right] A_c V_{ps} \tag{11}$$

For $\dot{F}$, we can write $\dot{F} = \dot{F}_b + \dot{F}_{gb}$, i.e. as the sum of the energy changes occurring in the grain bodies ($\dot{F}_b$) and the solid portion of the grain boundary zone ($\dot{F}_{gb}$). Here, $\dot{F}_b$ is the energy change due to mass removal from the grain bodies ($-2\bar{f}_b A_c V_{ps}$), plus the energy stored in mass precipitation on the pore walls ($+2\bar{f}_b A_p J_p$), so that, using Eqn. (8), gives:

$$\frac{\mathrm{d}F_b}{\mathrm{d}t} = \bar{f}_b \left(A_p J_p - 2A_c V_{ps}\right) = -\bar{f}_b A_c S \frac{\mathrm{d}\alpha}{\mathrm{d}t} \tag{12}$$

where $\bar{f}_b$ is the mean free energy density of solid stored in the grain body (units: $\mathrm{J\,m^{-3}}$). In turn:

$$\frac{\mathrm{d}F_{gb}}{\mathrm{d}t} = \frac{\mathrm{d}\left(\bar{f}_{gb}\nu^s_{gb}\right)}{\mathrm{d}t} = \bar{f}_{gb}\frac{\mathrm{d}\nu^s_{gb}}{\mathrm{d}t} + \nu^s_{gb}\frac{\mathrm{d}\bar{f}_{gb}}{\mathrm{d}t} \tag{13}$$

where $\bar{f}_{gb}$ is the mean free energy density of the solid in the perturbed grain boundary zone, and ν^s_{gb} is the volume of solid in the grain boundary zone. Clearly, from Fig. 1d, $\dot{\nu}^s_{gb} = A_c S\dot{\alpha}$. Using this relation, we combine Eqns. (12) and (13) to give:

$$\frac{\mathrm{d}F}{\mathrm{d}t} = \frac{\mathrm{d}F_b}{\mathrm{d}t} + \frac{\mathrm{d}F_{gb}}{\mathrm{d}t} = \left(\bar{f}_{gb} - \bar{f}_b\right) A_c S \frac{\mathrm{d}\alpha}{\mathrm{d}t} + \nu^s_{gb}\frac{\mathrm{d}\bar{f}_{gb}}{\mathrm{d}t} \tag{14}$$

In this relation, the first term on the right hand-side represents the excess solid energy stored in the grain boundary zone as the islands grow in volume, and the second corresponds to the change in grain boundary solid energy due to changing stress/strain concentrations in the evolving grain boundary structure.

The interfacial energy stored in the grain boundary zone is simply the sum $E_s = \gamma_{ss} A_c \alpha + 2\gamma_{sl} A_c \left(1 - \alpha\right)$ of solid-solid (ss) and solid-liquid (sl) interfacial energy (γ) terms (factor 2 accounting for the solid-liquid interfaces on both sides of the contact). This means that:

$$\dot{E}_s = \gamma_{ss} A_c \frac{\mathrm{d}\alpha}{\mathrm{d}t} - 2\gamma_{sl} A_c \frac{\mathrm{d}\alpha}{\mathrm{d}t} = \left(\gamma_{ss} - 2\gamma_{sl}\right) A_c \frac{\mathrm{d}\alpha}{\mathrm{d}t} \tag{15}$$

The solid-solid and solid-liquid surface energy terms are then related through the Young-Dupré relation (*Holness*, 1992) as given in Eqn. (4):

$$\gamma_{ss} = 2\gamma_{sl} \cos\frac{\theta_{eq}}{2} \tag{4 rev.}$$

Substitution of this relation into Eqn. (15) gives:

$$\dot{E}_s = -2\gamma_{sl}\left(1 - \cos\frac{\theta_{eq}}{2}\right) A_c \frac{\mathrm{d}\alpha}{\mathrm{d}t} = -2\gamma_{sl}\Delta\cos\frac{\theta}{2} A_c \frac{\mathrm{d}\alpha}{\mathrm{d}t} \tag{16}$$

Note that the definition of $\Delta\cos\left(\theta/2\right)$ is equivalent to that of *Visser* (1999) as given in Eqn. (5)

when $\theta = 0$, which is in full agreement with the idealised grain boundary geometry displayed in Fig. 1d.

From Eqn. (10), we hence obtain for the total dissipation:

$$\begin{aligned} \dot{\Delta} &= \dot{W} - \dot{F} - \dot{E}_s \\ &= 2\left[\sigma_c - P_f\right] A_c V_{ps} + \left[\frac{2\gamma_{sl}}{S}\Delta\cos\frac{\theta}{2} - \left(\bar{f}_{gb} - \bar{f}_b\right)\right] A_c S\frac{\mathrm{d}\alpha}{\mathrm{d}t} - \nu^s_{gb}\frac{\mathrm{d}\bar{f}_{gb}}{\mathrm{d}t} \end{aligned} \tag{17}$$

During active pressure solution with negligible inelastic deformation of the solid framework, this dissipation will be caused by the internal grain contact mass transfer process. Assuming that the rate of mass transfer is controlled by diffusion, then the dominant dissipative process will be radial grain boundary diffusion, with any internal short range diffusional dissipation being negligible. Hence, we can express the rate of dissipation for a radial increment $\mathrm{d}r$ due to radial diffusion as (*Lehner*, 1990; *Pluymakers and Spiers*, 2014):

$$\mathrm{d}\dot{\Delta} = -J_r a_p \frac{\partial\mu}{\partial r}\mathrm{d}r \tag{18}$$

where $a_p = 2\left(1-\alpha\right)S\pi r$ is the peripheral area at radius r that is open to the radial diffusive flux J_r. The diffusive flux is driven by a gradient in chemical potential μ, as given by Fick's first law:

$$J_r = -\frac{DC\Omega}{RT}\frac{\partial\mu}{\partial r} \tag{19}$$

Rewriting the solid mass balance Eqn. (8) for a grain boundary element explicitly for the diffusive flux, and substituting Eqn. (19) gives:

$$\begin{aligned} J_r = \frac{a_c}{a_p}\left(2V_{ps} - S\frac{\mathrm{d}\alpha}{\mathrm{d}t}\right) &= -\frac{DC\Omega}{RT}\frac{\partial\mu}{\partial r} \\ \Rightarrow \frac{\partial\mu}{\partial r} &= -\frac{RT}{DC\Omega}\frac{a_c}{a_p}\left(2V_{ps} - S\frac{\mathrm{d}\alpha}{\mathrm{d}t}\right) \end{aligned} \tag{20}$$

with $a_c = \pi r^2$ at radius r. Substituting Eqn. (20) into (18), and integrating over the grain contact area gives the final expression for $\dot{\Delta}$:

$$\begin{aligned} \dot{\Delta} &= \frac{DC\Omega}{RT}\int_0^{r_c} a_p\left(\frac{\partial\mu}{\partial r}\right)^2\mathrm{d}r \\ &= \frac{\pi}{2}\frac{RT}{DCS\left(1-\alpha\right)\Omega}\left(2V_{ps} - S\frac{\mathrm{d}\alpha}{\mathrm{d}t}\right)^2\int_0^{r_c} r^3\mathrm{d}r \\ &= A_c\frac{r_c^2}{8}\frac{RT}{DCS\left(1-\alpha\right)\Omega}\left(2V_{ps} - S\frac{\mathrm{d}\alpha}{\mathrm{d}t}\right)^2 \end{aligned} \tag{21}$$

Combining Eqn. (17) and (21), and noting from Fig. 1d that $\nu^s_{gb} = \left[w_{gb} - \left(1-\alpha\right)S\right]A_c$ (w_{gb} being

the width of the grain boundary zone), now leads to the result:

$$\begin{gathered} 2\left[\sigma_c - P_f\right] V_{ps} + \left[\frac{2\gamma_{sl}}{S}\Delta\cos\frac{\theta}{2} - \left(\bar{f}_{gb} - \bar{f}_b\right)\right] S\frac{\mathrm{d}\alpha}{\mathrm{d}t} - \\ \left[w_{gb} - (1-\alpha)\,S\right]\frac{\mathrm{d}\bar{f}_{gb}}{\mathrm{d}t} = \frac{r_c^2}{8}\frac{RT}{DCs\,(1-\alpha)\,\Omega}\left(2V_{ps} - S\frac{\mathrm{d}\alpha}{\mathrm{d}t}\right)^2 \end{gathered} \tag{22}$$

Assuming that the grain boundary zone is thin, so that $w_{gb} \to S$, it is reasonable to suppose that the main contribution to the excess free energy density in the grain boundary solid over the grain bodies, i.e. to $\left(\bar{f}_{gb} - \bar{f}_b\right)$, will be provided by the strain energy f_i stored in the highly loaded grain boundary islands. Taking this to be dominated by the elastic strain energy, we can write (c.f. *Van Noort et al.*, 2008):

$$\left(\bar{f}_{gb} - \bar{f}_b\right) \approx f_i = \frac{1}{2E}\left(\frac{\sigma_c}{\alpha}\right)^2 \tag{23}$$

where E is the Young's modulus of the solid. Writing $\bar{f}_{gb} \approx f_i + \bar{f}_b$ and noting that $\bar{f}_b$, the free energy density in the grain bodies, is constant at constant σ_c, it follows for $\mathrm{d}\bar{f}_{gb}/\mathrm{d}t$ in Eqn. (22) that:

$$\frac{\mathrm{d}\bar{f}_{gb}}{\mathrm{d}t} = \frac{\mathrm{d}f_i}{\mathrm{d}t} = \frac{\sigma_c^2}{2E}\frac{\mathrm{d}\left(\alpha^{-2}\right)}{\mathrm{d}t} = -\frac{\sigma_c^2}{E}\frac{1}{\alpha^3}\frac{\mathrm{d}\alpha}{\mathrm{d}t} \tag{24}$$

Putting these relations for $\left(\bar{f}_{gb} - \bar{f}_b\right)$ and $\mathrm{d}\bar{f}_{gb}/\mathrm{d}t$ into (22) and taking $w_{gb} \approx S$ now yields:

$$\begin{aligned} 2\left[\sigma_c - P_f\right] V_{ps} + \left[\frac{2\gamma_{sl}}{S}\Delta\cos\frac{\theta}{2} + \frac{1}{2E}\left(\frac{\sigma_c}{\alpha}\right)^2\right] S\frac{\mathrm{d}\alpha}{\mathrm{d}t} \\ = \frac{r_c^2}{8}\frac{RT}{DCS\,(1-\alpha)\,\Omega}\left(2V_{ps} - S\frac{\mathrm{d}\alpha}{\mathrm{d}t}\right)^2 \end{aligned} \tag{25}$$

For the steady-state case, when there is no evolution in grain boundary structure ($\dot{\alpha} = 0$), this relation reduces to the standard equation for pressure solution convergence velocity at a cylindrical grain contact (*Pluymakers and Spiers*, 2014):

$$V_{ps} = \frac{4DCS\,(1-\alpha)\,\Omega}{RTr_c^2}\left[\sigma_c - P_f\right] \tag{26}$$

When the pressure solution rate slows down to approach zero due to obstruction of radial diffusion with increasing α, i.e. as $V_{ps} \to 0$, Eqn. (25) reduces to:

$$S\frac{\mathrm{d}\alpha}{\mathrm{d}t} = \frac{8DCS\,(1-\alpha)\,\Omega}{RTr_c^2}\left[\frac{2\gamma_{sl}}{S}\Delta\cos\frac{\theta}{2} + \frac{1}{2E}\left(\frac{\sigma_c}{\alpha}\right)^2\right] \tag{27}$$

which expresses the rate of increase in contact area fraction occupied by islands of solid-solid contact under non-equilibrium conditions (compared with the condition for removal of an equilibrium grain boundary structure from equilibrium given by *Van Noort et al.* (2008). Note that Eqn. (27) describes the rate of island area increase during active pressure solution. The onset of static island growth is

still described by the equilibrium condition given by *Van Noort et al.* (2008) as:

$$\Delta\mu_i = \frac{2\gamma_{sl}}{S}\Delta\cos\frac{\theta}{2} - \frac{1}{2E}\left(\frac{\sigma_c}{\alpha}\right)^2 = 0 \qquad \text{(6 rev.)}$$

This equilibrium criterion marks an unstable fixed point, in that any value of σ_c/α above a critical value will cause nett contraction of the islands ($\Delta\mu_i < 0$), which in turn decreases α and farther removes the grain boundary from the equilibrium point. Similarly, once σ_c/α falls below a critical value determined by Eqn. (6) (i.e. $\Delta\mu_i > 0$), island growth causes σ_c/α to decrease further, continuing to remove the grain boundary farther from equilibrium. Initially, α will likely be small (of the order of a few per cent; *Van Noort et al.*, 2008), so that the onset of static island growth can only be reached by lowering σ_c by porosity reduction (compaction). It is therefore expected that there exists a critical aggregate porosity below which island growth initiates (*Van Noort et al.*, 2008).

Equation (25) is an ill-conditioned equation containing two unknowns, V_{ps} and $\dot{\alpha}$, and cannot be solved analytically without further constraints linking V_{ps} and $\dot{\alpha}$, beyond the end-member cases represented by Eqns. (26) and (27). In the absence of such constraints, and noting the numerous simplifications and approximations made in deriving Eqn. (25) for V_{ps} and $\dot{\alpha}$, a first-order solution to acquiring V_{ps} and $\dot{\alpha}$ can be obtained by assuming that at any instant the pressure solution process and the tendency for islands to increase in area operate independently. In line with this, we take the rate of pressure solution at an evolving grain contact to be given by Eqn. (26) at any instant, with α evolving with time according to Eqn. (27).

3.2 Grain boundary connectivity

It was mentioned in Section 2 that the connectivity and diffusive properties of a grain boundary depend on the structure of the grain contact. The evolution of the grain boundary as described by the above model formulations must therefore be reflected by the transport properties of the grain boundary, which we will detail below.

Several microstructural studies have shown that healed grain boundaries contain arrays of fluid inclusions in the form of isolated spheres or tubes (e.g. *Desbois et al.*, 2012; *Hickman and Evans*, 1991; *Urai et al.*, 1986). In grain boundaries that show a lesser degree of healing, these tubes connect up with neighbouring inclusions to form a network that connect the interior of the grain boundary to the pore space (*Ghoussoub and Leroy*, 2001; *Spiers and Schutjens*, 1990). Also finer scale structures can be observed, possibly related to local lattice defects (*Schenk and Urai*, 2004; *Schutjens and Spiers*, 1999). If the density of inclusions, tubes, and pits is high enough, they can provide an interconnected pathway from the centre of the grain boundary into the pore space. In general, this will apply both to a statically healing grain boundary, but also to a dynamically wetted grain boundary island-channel structure undergoing progressive structural evolution during pressure solution. To estimate the probability that a given location within the grain boundary is connected to the pore space, and to quantify how the transport properties of the grain boundary change with asperity size and area fraction, we employ percolation theory, following standard percolation theory

formulations (see *Stauffer and Aharony*, 1992).

In this framework, any random location in the grain boundary rim is assigned an 'open' or 'closed' state. In our current view of a grain boundary, the open state corresponds to a channel, and is open to the diffusive mass flux. The closed state can be seen as an asperity (solid-solid) contact. The probability p of a site being open is related to the relative asperity contact area α as:

$$p = \frac{A_{sl}}{A_c} = \frac{A_c\,(1-\alpha)}{A_c} = 1 - \alpha \tag{28}$$

The probability of a site being closed is then $(1-p) = \alpha$. It can be shown that in an infinitely large system, clusters of open sites that traverse the entire length of the system exist (i.e. percolation occurs) only when $p > p_c$. The value of p_c can be calculated (analytically or numerically) for various geometries, or, in the current situation, can be estimated from microstructural estimates of α in the fully-sealed state (so that $p_c = 1 - \alpha_c$), assuming that mass and fluid transport do not proceed once a contact has fully healed (with the term 'healing' loosely referring to the progression of asperity growth, c.f. *Van Noort et al.*, 2008). Furthermore, numerous universal scaling relations have been derived that describe transport properties of the system. For instance, the effective diffusivity of a system of infinite size can be expressed as:

$$D^{eff} \propto (p - p_c)^{\nu} \tag{29}$$

Here, ν assumes a value of 1.16 in 2D (*Sahimi*, 2003). To determine the proportionality constant, we assume that in the initial, unhealed state, $\alpha = \alpha_0$, $p = p_0 = 1 - \alpha_0$, and $D^{eff} = D^0$, so that (29) becomes:

$$D = D^{eff} = D^0 \left(\frac{[p - p_c]}{[p_0 - p_c]} \right)^{\nu} = D^0 \left(\frac{\alpha_c - \alpha}{\alpha_c - \alpha_0} \right)^{\nu} \tag{30}$$

Note that we implicitly assume that the system is infinite in size, which is a valid approximation when the size of the grain-grain contact far exceeds the characteristic size of an open site (etch pit, fluid inclusion, or tube size). In the case where this assumption is not valid, the percolation threshold p_c is expected to decrease in magnitude, and percolation of the system is more likely. Additional scaling can be performed to better represent percolating clusters of finite size (see *Stauffer and Aharony*, 1992).

As the asperities increase in size, α increases towards α_c and p approaches p_c. For $p \leq p_c$ (and equivalently $\alpha \geq \alpha_c$), no percolation occurs and the grain boundary is said to to be fully healed and sealed, effectively terminating pressure solution. Mass transfer may still occur internally to restructure the island-channel network, breaking up the network in tubes and isolated fluid inclusions (*Brantley*, 1992). During this, the proportion of fluid stored in the grain boundary is thought to remain unchanged. Based on microstructural accounts of healed grain boundaries (see e.g. *Desbois et al.*, 2012; *Ghoussoub and Leroy*, 2001; *Schutjens*, 1991; *Urai et al.*, 1986), we estimate that the grain contact surface area occupied by solid falls between 0.5 and 0.8, which bounds the range of values for α_c. The value of p_0 is estimated to exceed 0.9, corresponding to $\alpha_0 < 0.1$, as suggested by *Renard et al.* (2012) and *Van Noort et al.* (2008), although it can be argued that near the onset of progressive

grain boundary island growth, α attains higher values (*Van Noort et al.*, 2008). Taking then values of p_0, p_c, α_0, and α_c, and using Eqn. (27) to describe $\dot{\alpha}$, Eqn. (30) now provides a description of the evolution of D^{eff}.

It is evident how a moderation of the transport properties of the grain boundary can result in a reduction of the rate of pressure solution, if it is limited by the rate of diffusion (like for halite at room temperature). In the case that the rate of pressure solution is controlled by the interface reaction rate (like for quartz in the experiments of *Niemeijer et al.*, 2002), the influence of an evolving grain boundary structure will only manifest itself in the overall pressure solution rate when D^{eff} has been reduced sufficiently for the process to become controlled by the rate of diffusion. In other words, a switch in rate-limiting process is anticipated in materials for which pressure solution is initially interface-reaction controlled.

3.3 Scale-dependence of grain boundary topography

Throughout this section, it has been assumed that the average grain boundary roughness S is time- and scale-invariant. However, it cannot be excluded that this roughness is dependent on the size of the contact, or on grain boundary stress (c.f. *Schutjens and Spiers*, 1999). We will explore this possibility in more detail by considering a scale-dependence of S.

It has been suggested in numerous studies that (dynamic) interfaces are self-affine, including natural faults and joints (*Brodsky et al.*, 2016; *Brown and Scholz*, 1985; *Candela et al.*, 2012), stylolites (*Gratier et al.*, 2005; *Renard et al.*, 2004), processed or naturally corroded metal surfaces (*Majumdar and Tien*, 1990; *Shanhua et al.*, 2015; *Zahouani et al.*, 1998), and various geomaterials (*Avnir et al.*, 1984; *Dieterich and Kilgore*, 1996; *Wong et al.*, 1986). Owing to its self-affine character, a given surface will appear smoother at larger length-scales. When it is assumed that the average thickness of a grain boundary is controlled by its roughness, then self-affinity implies that $S \propto L^H$, where L is a characteristic length scale (i.e. the size of the contact), and H is the Hurst exponent (with $H \neq 1$ for self-affine surfaces; *Brodsky et al.*, 2016). A dynamically evolving grain boundary may not obey such a scaling law, as the topography may be strongly controlled by fluid-rock interactions. However, a size-dependent topography is well established for stylolites over 4-5 orders of magnitude (see *Gratier et al.*, 2013, and references therein), and has previously been reported for grain interfaces undergoing pressure solution at the μm-scale (*De Meer et al.*, 2002, 2005; *Schutjens and Spiers*, 1999). *De Meer et al.* (2005) report that the average grain boundary thickness increases with increasing contact width. This can also be inferred from the observed increase in kinetic constant DCS with increasing contact width (*De Meer et al.*, 2002), assuming that D and C are scale-independent. Furthermore, *Schutjens and Spiers* (1999) observed contact roughness at all resolvable scales, ranging from tens of μm to a few hundred nm, suggesting a fractal topography. Finally, stressed interfaces deforming by elastic and/or plastic yield are well characterised by a fractal relationship (*Brown and Scholz*, 1985; *Dieterich and Kilgore*, 1996).

Since the chemical potential for asperity growth (or undercutting) depends strongly on S (see

Eqn. (27)), the possibility that S scales with contact size needs to be considered. Therefore, we define S to vary with r_c, following a power-law scaling relationship, in line with our preceding discussion of such effects. More specifically:

$$S = S^{ref} \left(\frac{r_c}{r_c^{ref}} \right)^H \tag{31}$$

Here, S^{ref} is a reference value corresponding to a radius of contact r_c^{ref}, and H is the Hurst exponent. A value of $H = 0$ results in a scale-independent (constant) value of S. Using this relation, the asperity growth rate as predicted by Eqn. (27) is altered through the surface energy term, which contains S in the denominator. For consistency, the value of S as appearing in the experimentally determined product DCS in Eqn. (1b) is also scaled using the above relation, so that both the rate of pressure solution and that of asperity growth are affected by the simulated changes in topography. When scaling DCS, we assume that the experimentally determined value of this product corresponds to DCS^{ref}, so that the product scales as $DCS^{ref} \left(r_c / r_c^{ref} \right)^H$. Note that Eqn. (31) is purely empirical in nature, and therefore has little predictive power. However, we will only use this relationship to investigate the possible effects of a scale-dependent contact roughness on the grain boundary island growth behaviour, by comparing simulations with constant S to those where S is scaled.

3.4 Analytical model for pressure solution with grain boundary evolution

Classically, the constitutive relations for pressure solution creep are derived for a single contact, before being up-scaled to the size of the (porous) aggregate, assuming an average unit-cell geometry and stress distribution (see e.g. *Pluymakers and Spiers*, 2014; *Rutter*, 1976; *Spiers and Schutjens*, 1990). For obtaining a description of pressure solution with grain boundary evolution analytically, we adopt classical treatments of the model aggregate by assuming a well-defined relationship between bulk porosity and the area (or equivalent radius) of an individual grain-grain contact. This relationship reads (*Pluymakers and Spiers*, 2014):

$$r_c = d\sqrt{\frac{F}{\pi Z} f(\phi)} \tag{32}$$

Here, F is a shape factor that assumes a value of π for spherical grains, and Z is the bulk-average coordination number. $f(\phi)$ is a smooth function that describes the evolution of contact area with porosity, and is chosen such that $f(\phi_0) = 0$ and $f(0) = 1$. C.f. *Spiers et al.* (2004), we define $f(\phi)$ as:

$$f(\phi) = \frac{\phi_0 - \phi}{\phi_0} \tag{33}$$

In this expression, ϕ_0 roughly corresponds to the porosity at the start of the experiment, where the area of contact of grains is relatively small. Using relation (32), the constitutive equations (26) and (27) can then be up-scaled from a single grain-grain contact to an assembly of packed grains to give:

$$\dot{\varepsilon} = 4\pi A_\varepsilon \left(\frac{Z}{F}\right)^2 \frac{DCS\,(1-\alpha)\,\Omega}{RT} \frac{\sigma_e}{d^3 f(\phi)^2} \tag{34a}$$

$$\frac{\mathrm{d}\phi}{\mathrm{d}t} = -\,(1-\phi)\,\dot{\varepsilon} \tag{34b}$$

$$\frac{\mathrm{d}\alpha}{\mathrm{d}t} = 8\pi \frac{Z}{F} \frac{DC\,(1-\alpha)\,\Omega}{RTd^2 f(\phi)} \left(\frac{2\gamma_{sl}}{S}\Delta \cos\frac{\theta}{2} + \frac{1}{2E}\left[\frac{Z}{F}\frac{\sigma_e}{\alpha f(\phi)}\right]^2\right) \tag{34c}$$

Here, A_ε is a geometric factor that assumes a value of 6 for isotropic compaction. D is modified by α through Eqn. (30) and S through Eqn. (31). The full set of coupled differential equations (Eqn. (34)), complemented with Eqn. (30) and (31), is solved iteratively using the *SciPy* ODE package (*Jones et al.*, 2001) to yield the evolution of D, α, strain rate, strain and porosity with time.

4 Analytical model predictions versus experiments on halite

Here, we compare the deformation rates measured by *Schutjens* (1991) in long-term compaction experiments with the results of our extended model for pressure solution plus grain boundary evolution as expressed by Eqn. (34). For this comparison, we require laboratory data from high-strain ($\phi < 15$ %) compaction tests performed under conditions for which diffusion-controlled pressure solution is the dominant deformation mechanism, limiting the contribution of e.g. microcracking to the overall rate of compaction. Moreover, the kinetics of pressure solution need to be well constrained, so that uncertainties in the model constitutive parameters can be excluded to contribute to discrepancies between the laboratory data and model predictions. To our best knowledge, only the data set reported by *Schutjens* (1991) satisfies these specific criteria, and so we will compare our model outcomes to this data set.

We start by comparing the predictions of grain boundary evolution (Eqn. (34)) for a constant value of S with the laboratory data of *Schutjens* (1991) (see Fig. 2 – constructed from his Fig. 3.14). This comparison is made for each experiment individually – see Fig. 3. The parameters used in the analytical models are given in Table 1. First, we examine a model that does not consider grain boundary evolution, i.e. using Eqn. (34) with $\dot{\alpha} = 0$, so that α and D are constant. At high porosities, there is acceptable agreement between the strain rates predicted by the model and measured in the experiments, but for porosities <25 % the analytical model starts to overestimate the compaction rates. Near the terminal porosity of the experiments the mismatch between model and experimental strain rates is up to several orders of magnitude, illustrating that the existing theory of pressure solution does not describe the compaction behaviour at porosities below 20 %.

Next, we consider a model where the grain boundary structure evolves, with $\dot{\alpha}$ being described by Eqn. (34c), and D being modified by the instantaneous value of α in accordance with Eqn. (30). The comparison between the experimental data and model predictions including grain boundary evolution (Fig. 3) shows that when a constant value of $S = 325$ nm is taken, only the data for a grain size

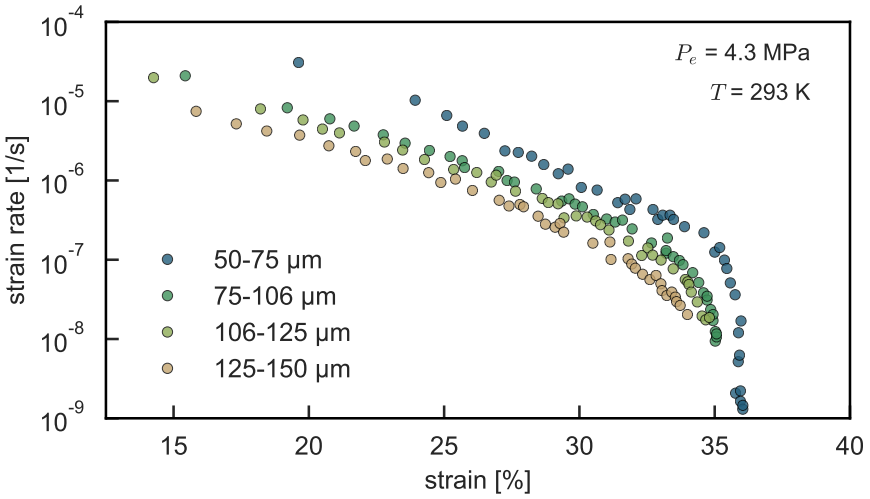

Figure 2: Digitised results of the isostatic compaction experiments on NaCl reported by *Schutjens* (1991). The experiments were performed at room temperature conditions, and the test samples were subjected to a servo-controlled effective pressure of 4.3 MPa.

range of 125-150 µm can be accurately represented by the model (Fig. 3d), while for all other grain size ranges, the model overestimates experimental compaction rates and underestimates the terminal porosity. Although the model with constant S broadly displays the same features as the experimental data, the fit between the analytical models and compaction data is much improved by allowing S to evolve with the size of the grain contact (Eqn. (31)), suggesting a scale dependence of S as discussed in Section 3.3. However, it should be noted that in the analytical model approach, up-scaling from the grain contact scale to that of the aggregate (i.e. relating mean grain contact size to porosity) involves an empirical porosity function $f(\phi)$. While this has been shown to be accurate for a wide porosity range (*Niemeijer et al.*, 2002; *van den Ende et al.*, 2018; *Zhang et al.*, 2010), it cannot be excluded that the apparent scale dependence of S stems from the functional form of $f(\phi)$, which may not accurately represent the evolution of grain contact area and coordination number with porosity in the experimental samples at lower porosities. Additionally, the polydispersed (multi-valued) distribution of grain sizes in the laboratory aggregates, as well as the presumed circular contact geometry, may affect the apparent scale dependence of S.

Finally, we compare two models that consider a scale dependence of $S \propto r_c^H$, with Hurst exponents $H = 0.5$ and $H = 1.1$ as suggested by roughness measurements of natural stylolites (e.g. *Renard et al.*, 2004) – see Fig. 4. From the comparison, it is evident that the overall compaction rates are sensitive to the value of H, and that the laboratory data can only be explained by a model with a Hurst exponent of 0.5.

Parameter	Value	Units
Nominal grain diameter	62.5, 90.5, 115.5, 137.5	µm
Effective pressure (P_e)	4.3	MPa
Initial porosity (ϕ_0)	40.0	%
Geometric constant (A_ε)	6	-
Grain shape factor (F)	π	-
Grain coordination number (Z)	6	-
Kinetic constant (DCS)	1.22×10^{-19}[a]	$m^3\ s^{-1}$
Molar volume (Ω)	2.69×10^{-5}	$m^3\ mol^{-1}$
Temperature (T)	294	K
Surface energy (γ_{sl})	0.2[b]	$J\ m^{-2}$
Dihedral angle mismatch ($\Delta \cos \frac{\theta}{2}$)	0.18[c]	-
Asperity Young's modulus (E)	37	GPa
Initial asperity occupation ratio (α_0)	0.15	-
Terminal asperity occupation ratio (α_c)	0.8	-
Reference grain boundary thickness (S^{ref})	325	nm
Reference contact radius (r_c^{ref})	35	µm
Hurst exponent (H)	0.5	-

Table 1: Parameters used in the analytical model simulations. The sequence of grain sizes above correspond to the mean of the grain size ranges of experiments L1, L2, L3, and L4 respectively, as reported by *Schutjens* (1991). References: a) *Spiers et al.* (1990); b) *Visser* (1999) using the approximation by *Israelachvili* (1986); c) *Lewis and Holness* (1996).

5 Discussion

The analytical model has been compared with laboratory data for isostatic compaction of NaCl aggregates, as reported by *Schutjens* (1991). The comparison shows good agreement regarding the trends in densification rates, demonstrating that grain boundary evolution involving an increase in solid-solid contact area associated with a decrease in surface energy can explain the retardation of pressure solution creep rates. In spite of the good quantitative match between the laboratory data and the models, a number of issues remain unresolved. Most notably, the structure and dynamics of a wetted grain boundary, and its relation to pressure solution, require further discussion. In addition, the relevance and implications of the present findings for pressure solution in nature requires examination. These topic will be addressed in the following sections.

5.1 Structure and dynamics of a wetted grain contact under stress

In classical analytical treatments of steady-state pressure solution (e.g. *Lehner*, 1995; *Spiers and Schutjens*, 1990; *Pluymakers and Spiers*, 2014), the smallest scale that is explicitly considered encompasses a segment of a grain contact over which a representative average grain boundary structure can be assumed. The local dynamics of grain contact structure is not made explicit in these models. Instead, a fixed, steady-state structure is assumed. However, for a rigorous investigation of the evolution of the structure of a wetted grain boundary under stress, this local scale needs to be considered explicitly, without assuming steady-state. In our analysis presented in Section 3.1, we

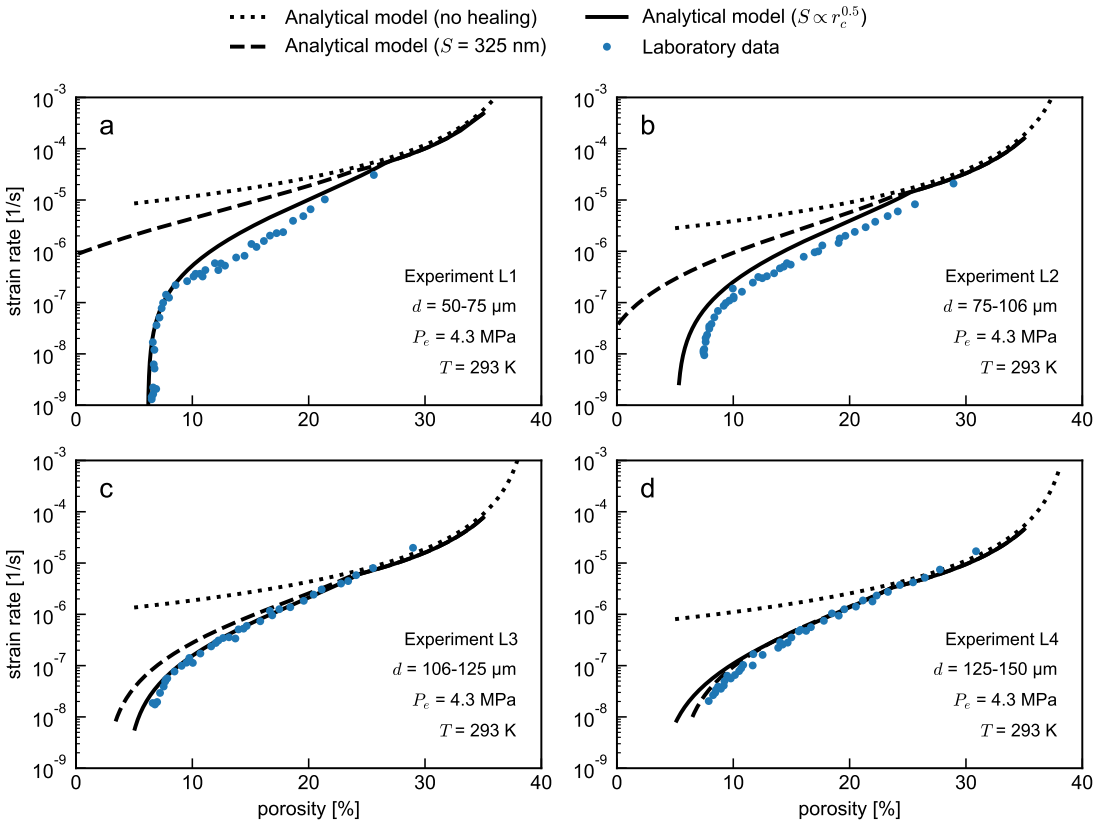

Figure 3: Comparison between analytical models and the laboratory results of *Schutjens* (1991). For each laboratory data set, three model results are shown: one where no grain boundary evolution is considered (i.e. Eqn. (34) with $\dot{\alpha} = 0$), one where grain boundary evolution is considered with a constant value of $S = 325$ nm, and one where grain boundary evolution is considered with $S \propto r_c^H$ and $H = 0.5$. Experimental parameters are as indicated in each panel.

made a number of simplifying assumptions regarding the distribution of the local free energy and the structure of the grain boundary zone. These assumptions were required in order to derive closed-form expressions for the structural evolution of the grain boundary, given our present knowledge on the processes that control the dynamics of dissolution, diffusion, and precipitation at the scale of a single island.

An important gap in our knowledge remains the lack of a quantitative description of the processes that cause the grain boundary to remain dynamically rough when subjected to a sufficiently high state of stress. See-through experiments (*Schutjens and Spiers*, 1999) demonstrate that an optically flat interface undergoing pressure solution can regenerate a rough topography when the stress supported by the interface is raised. Such behaviour is not reflected by our present model describing grain boundary evolution (Eqn. (27)). Closely related to these observations, is the possibility that the grain boundary roughness, and correspondingly the mean thickness S of the interstitial fluid film, are scale-dependent. In-situ spectroscopy experiments performed by *De Meer et al.* (2005) on a single

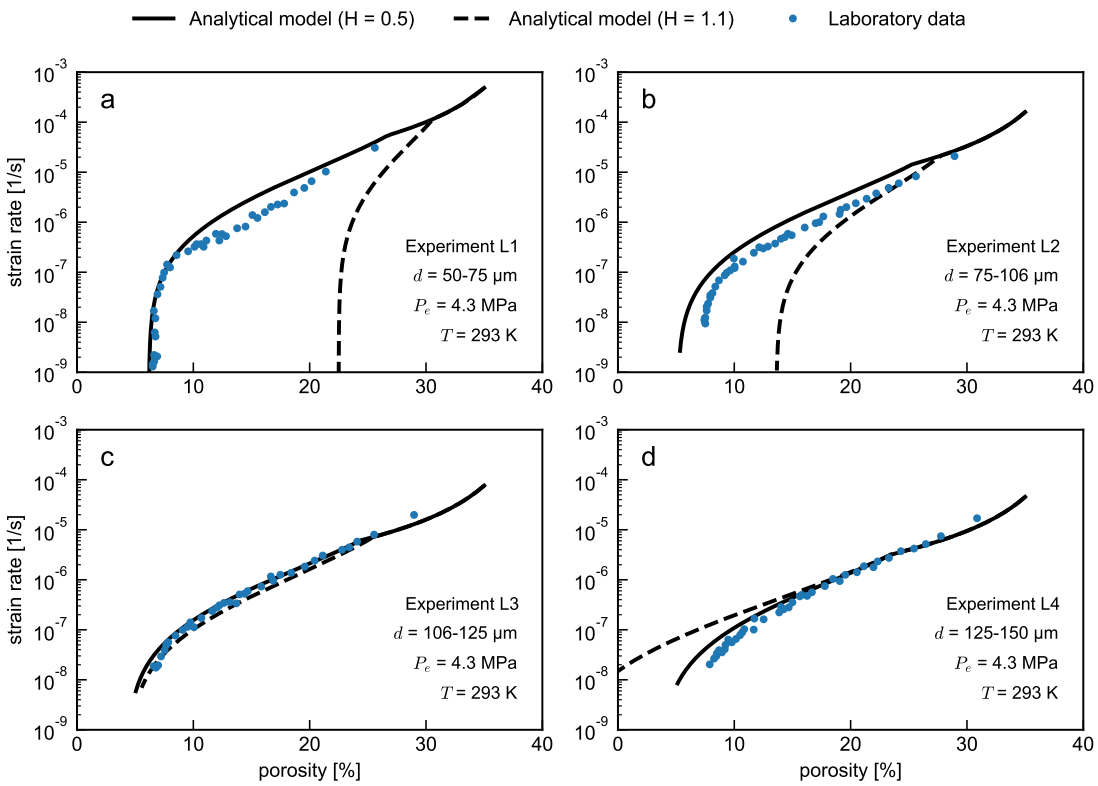

Figure 4: Comparison between analytical models and the laboratory results of *Schutjens* (1991). For each laboratory data set, two model results are shown: one where where grain boundary evolution is considered with $S \propto r_c^H$ and $H = 0.5$ (solid line), and one with $H = 1.1$ (dashed line). Experimental parameters are as indicated in each panel.

grain contact revealed that S increases over time, concurrent with widening of the stressed interface. However, it is presently not clear whether this is a transient effect, or if a steady-state value of S is attained for a constant size of the contact.

In the context of the topographic evolution of stylolites, *Renard et al.* (2004) (see also *Schmittbuhl et al.* (2004)) proposed a Langevin model describing the growth of stylolites as a competition between stress-induced roughening and surface-energy driven smoothening, in the presence of stochastic noise (e.g. spatiotemporal heterogeneity in dissolution kinetics). This model predicts an effective Hurst exponent of $H = 1.2$ at small length scales, and $H = 0.4$ at large length scales, corresponding with the dominance of either stress or surface energy in controlling the dynamics of the system, respectively. The transition from one regime to the other is governed by a characteristic length scale l_c, given as:

$$l_c = \frac{E\gamma_{sl}}{2\sigma_0^2\,(1-\nu^2)} \tag{35}$$

where σ_0 is the normal stress acting across the stylolite dissolution plane, and ν is the Poisson ratio of the solid. The predicted values of the Hurst exponent and the interpretation of l_c were found to be in

good agreement with measurements of the Hurst exponent for natural stylolite samples, which were characterised by end-member Hurst exponents of $H = 0.5$ and $H = 1.1$. By interpreting a stressed grain contact undergoing pressure solution as a 'microstylolite', the corresponding value of the Hurst exponent (either 0.5 or 1.1) can be estimated based on the magnitude of l_c relative to the size of the grain contact. Substitution of $E = 37$ GPa, $\gamma_{sl} = 0.2$ J m^{-3}, $\sigma_0 = \sigma_c = 20$ MPa, and $\nu = 0.25$ yields a characteristic length scale $l_c = 10$ µm, which is smaller than the mean grain contact size (being of the order of the grain size). This estimation suggests that on the scale of the grain contacts, long-range stress effects dominate the dynamics and accordingly the Hurst exponent assumes a value of 0.4-0.5, in agreement with the estimated value of $H = 0.5$ in the simulations.

Following the reasoning above, it can be argued that materials other than halite (e.g. calcite) will exhibit similar values of l_c at a given value of stress, as l_c is only linearly dependent on the material/interface properties (E, γ_{sl}). On the other hand, the effective contact stress exerts a quadratic control on l_c, and so the model of *Renard et al.* (2004) predicts a strong sensitivity of the grain contact Hurst exponent on porosity, fluid pressure, and applied stress. Furthermore, for aggregates exhibiting small grain sizes of the order of micrometres (such as for fault gouges), the grain contact size will generally be much smaller than l_c, so that compaction of such aggregates is expected to be governed by a Hurst exponent in the range of 1.1-1.2. As can be seen in Fig. 4a, such an increase in Hurst exponent dramatically diminishes the rate of compaction by pressure solution for small grain sizes. Laboratory measurements of compaction of coarse-grained aggregates may therefore not be representative for those of fine-grained aggregates.

5.2 Relation between grain boundary evolution and intergranular pressure solution

When considering static island growth driven by surface energy (e.g. *Van Noort et al.*, 2008), each individual island may have an unconstrained (infinite) lifetime, in that it may grow without being completely removed by dissolution over the lifetime of the grain contact. However, in order to achieve grain convergence when pressure solution operates, it is required that the entire grain boundary zone fully dissolves and rejuvenates its islands in a finite amount of time. If this were not the case, i.e. if islands would not fully dissolve, then nett dissolution would only occur by deepening of the channels (increasing S), which does not produce grain convergence. As a corollary, the lifetime of each individual island must be finite (i.e. it must fully dissolve), and new islands must form by non-uniform dissolution and compression of the grain contact, if pressure solution were to operate. This provokes a paradoxical interpretation of the grain boundary evolution model described in Section 3: an increasing value of α (the area fraction occupied by islands) seems suggestive of growth of individual islands, similar to the case of static island growth with no pressure solution. However, α reflects a spatial average of the total area occupied by islands, rather than describing the size and shape of individual islands. During active pressure solution, the nett rate of dissolution of islands may be reduced (induced by local changes in free energy) compared to the rate of formation of islands, resulting in a nett increase in α, even though islands still exhibit a finite lifetime.

Although it is explicitly assumed in the model derivation of Section 3.1 that pressure solution is operative during (dynamic) grain boundary evolution, it can be questioned whether this assumption is valid, or whether pressure solution is immediately arrested as soon as the nett volume occupied by islands starts to increase (static growth). A number of optical imaging experiments report negligible convergence during growth of interface asperities (*Renard et al.*, 2012), or of the stressed contact between a plano-convex lens pressed against a flat plate (*Hickman and Evans*, 1991, 1992; *Beeler and Hickman*, 2015), under conditions favourable for pressure solution. These observations suggest that pressure solution does not operate during structural evolution of the grain contact. However, as was noted by *Schutjens and Spiers* (1999), the plano-convex geometry employed in the experiments of *Hickman and Evans* (1991, 1992) (and of *Beeler and Hickman*, 2015) promotes contact growth due to the large radius of curvature at the contact margin. In the experiments of *Renard et al.* (2012), the nominal contact stress was low (0.26 MPa), and the contact asperities large in size (up to 300 µm). These experiments may therefore not be representative for our envisioned dynamic island-channel structure at the scale of tens to a few hundred nm.

In optically monitored grain-to-grain contact experiments conducted by *Schutjens and Spiers* (1999), all experiments showed convergence concurrent with an evolving grain boundary structure. Particularly, their experiment T4 displayed a gradual smoothing of an initially rough grain contact over the course of 25 days, until an optically smooth interface topography was achieved. Upon step-wise increasing the load on the contact, the grain contact re-roughened and the initial roughness was recovered (see Fig. 10 in *Schutjens and Spiers*, 1999). This example illustrates that pressure solution can continue to operate during grain boundary evolution.

5.3 Implications of the present findings for pressure solution in nature

We have established that grain boundary evolution may significantly retard pressure solution creep rates in mono-mineralic aggregates at high volumetric strains and low porosities (< 20 %). Our models for pressure solution concurrent with grain boundary evolution have been compared with isostatic compaction data on halite, which has previously been adopted in laboratory tests as an analogue material for quartz at hydrothermal conditions (*Niemeijer et al.*, 2009; *Bos et al.*, 2000). Although the material properties of halite are dissimilar from those of quartz, the processes involved in deformation of halite aggregates (e.g. pressure solution), have similarly been recognised to operate in quartz aggregates at the relevant conditions (*De Boer et al.*, 1977; *van Noort et al.*, 2008; *Heald*, 1955). This notion receives further support from the high-strain compaction tests performed on quartz by *Niemeijer et al.* (2002), reporting similar compaction trends at temperatures in the range of 400-600 °C as have been observed by *Schutjens and Spiers* (1999) in halite at room temperature conditions. Even though the process that limits the rate of pressure solution at high porosities is different for halite at room conditions than it is for quartz at hydrothermal conditions (diffusion versus dissolution, respectively; *Schutjens and Spiers*, 1999; *Niemeijer et al.*, 2002), it is expected that diffusion will become rate-limiting for both materials at low porosities (see Section 3.2). The models for pressure solution and grain boundary evolution derived in this study may therefore generally

apply to other materials, in a laboratory setting as well as in nature.

In contrast to many laboratory tests performed on mono-mineralic aggregates, natural sediments and fault gouges are often heterogeneous in composition. Given that solid-liquid and solid-solid interface energies play an important role in controlling the structural evolution of grain boundaries, the efficiency of grain boundary evolution as envisioned in this work can be challenged. A reduced efficiency of grain boundary evolution driven by surface energy has been observed in several laboratory experiments:

- *Beeler and Hickman* (2015) observed that quartz-sapphire interfaces of compressed plano-convex lenses do not show grain contact spreading (neck growth), in contrast to quartz-quartz interfaces. Similarly, the inhibiting effect of bi-mineral interfaces was inferred from the difference in convergence rates measured in experiments conducted on halite-halite and halite-silica interfaces (*Hickman and Evans*, 1991).
- *Hickman and Evans* (1992) showed that neck growth is faster for mono-mineralic interfaces with a lower crystallographic misorientation.
- Lastly, in the compaction experiments of *Zubtsov et al.* (2004), pure halite aggregates displayed lower compaction rates than mixtures of halite and calcite, even though calcite is characterised by slower pressure solution kinetics than halite. This behaviour was attributed to a reduced efficiency of healing of halite-calcite interfaces, and correspondingly the inhibition of retardation of pressure solution as compared to pure aggregates.

These observations suggest that the potential for grain boundary evolution is reduced by the solid-liquid and solid-solid interfacial energies associated with an incompatible bi-mineral configuration, or possibly by a strong contrast in dissolution or precipitation rates of each of the minerals in contact. This has implications for the compaction behaviour of poly-mineralic aggregates in nature: relatively pure (mono-phase) aggregates may experience significant retardation in pressure solution creep rates at low porosities, whereas mixed, poly-phase aggregates may not. This effect is noticeable when comparing densification rates of single-phase aggregates with poly-phase aggregates in laboratory compaction tests (e.g. *Niemeijer and Spiers*, 2002; *Zubtsov et al.*, 2004).

The operation (or absence) of grain boundary evolution hold important implications for the time-dependent restrengthening of faults. It is generally acknowledged that faults densify during interseismic times, for which pressure solution creep is an important mechanism at in-situ conditions (*Chester and Chester*, 1998; *Evans and Chester*, 1995; *Holdsworth et al.*, 2011; *Smeraglia et al.*, 2017). The compaction of faults is thought to contribute to the restrengthening of a fault after a seismic event (*Angevine et al.*, 1982; *Sleep and Blanpied*, 1992; *Yasuhara et al.*, 2005), and so faster compaction rates would result in a larger build-up of frictional strength over a seismic cycle. If grain boundary evolution operates efficiently, compaction and frictional restrengthening by pressure solution may be severely inhibited. On the other hand, it was remarked by *Hickman and Evans* (1991) that healed interfaces exhibit significant cohesive strength, and so grain boundary evolution may contribute to the total fault strength by time-dependent cohesion, complementing restrengthening due to compaction

by pressure solution. Naturally, this time-dependent strengthening mechanism requires that the structure of the grain boundaries be unperturbed by contact renewal processes such as granular flow, contributing to the competition between time-dependent strengthening and slip-dependent weakening (e.g. *Chen and Spiers*, 2016). In fault gouges of poly-mineralic composition (particularly when phyllosilicates are abundant) restrengthening by compaction is promoted, but restrengthening by time-dependent cohesion may be negligible if grain boundary island growth is the sole mechanism for generating cohesion. This presents opportunities for future research, and an application of the models developed in this work in the context of fault- and earthquake mechanics.

6 Conclusions

In this study, we have derived expressions that describe the evolution of the grain boundary structure within stressed grain contacts undergoing pressure solution. We have focussed on the interplay between growth in asperity contact area and pressure solution creep and the ultimate cessation of pressure solution when the grain boundary fluid connectivity breaks down, in the approach to the percolation threshold. The resulting analytical relations describing the rate of pressure solution and of the increase in grain boundary solid contact area at individual grain contacts have been used to predict aggregate behaviour, assuming a uniform pack of identical grains to up-scale contact behaviour to the aggregate scale. The compaction behaviour of granular aggregates as predicted by our new model has been compared with the (only suitable) compaction experiments on NaCl conducted by *Schutjens* (1991). From this comparison, we conclude the following:

1. Overall, grain boundary evolution involving asperity growth can explain the large reduction in pressure solution strain rates with decreasing porosity seen in experiments. The discrepancy between experimental compaction rates and predictions from analytical models that do not include grain boundary evolution (i.e. when the grain boundary structure and effective diffusivity are constant) can be fully accounted for when an evolving grain boundary structure and fluid channel constriction are considered.

2. When a constant value for the grain boundary thickness (S) is assumed, the predicted strain rates do not compare well with the full laboratory data set. Rather, model results with constant S only compare well for a single specific grain size range, suggesting that the grain size dependence is not captured properly. However, when S is assumed to scale with the size of the contact, corresponding to a self-affine grain boundary topography, the entire data set can be modelled with a single set of parameters. While this does not prove that S is scale-dependent, it does suggest that actively dissolving interfaces may display a fractal geometry, in line with previous observations on stylolite interfaces. To further validate the model, the characteristics of such interfaces need to be better constrained.

3. The new models for pressure solution concurrent with grain boundary evolution provide means to investigate long-term compaction behaviour of relatively pure (mono-phase) natural aggregates under in-situ conditions. However, the driving force for grain boundary evolution provided

by differences in solid-solid and solid-liquid surface energy may be diminished or absent bi-mineral interfaces, so that poly-phase aggregates may not exhibit a pronounced retardation of pressure solution creep rates as seen in mono-phase aggregates. This is of particular interest to the investigation of interseismic restrengthening of gouge-filled faults, which often feature a heterogeneous mineralic composition.

Our model for pressure solution concurrent with structural evolution of the grain boundary provides new insights into the process of pressure solution, and demonstrates the relevance of explicitly considering the structure of a wetted grain contact under stress. This warrants future research into the structure dynamics and evolution of grain boundaries in stressed fluid-rock systems in greater detail.

References

Angevine, C. L., D. L. Turcotte, and M. D. Furnish (1982), Pressure solution lithification as a mechanism for the stick-slip behavior of faults, *Tectonics*, *1*(2), 151–160, doi:10.1029/TC001i002p00151.

Avnir, D., D. Farin, and P. Pfeifer (1984), Molecular fractal surfaces, *Nature*, *308*(5956), 261–263, doi:10.1038/308261a0.

Beeler, N. M., and S. H. Hickman (2015), Direct measurement of asperity contact growth in quartz at hydrothermal conditions, *Journal of Geophysical Research: Solid Earth*, *120*(5), 3599–3616, doi:10.1002/2014JB011816.

Blanpied, M. L., D. A. Lockner, and J. D. Byerlee (1992), An earthquake mechanism based on rapid sealing of faults, *Nature*, *358*(6387), 574–576, doi:10.1038/358574a0.

Bos, B., C. J. Peach, and C. J. Spiers (2000), Slip behavior of simulated gouge-bearing faults under conditions favoring pressure solution, *Journal of Geophysical Research: Solid Earth*, *105*(B7), 16,699–16,717, doi:10.1029/2000JB900089.

Brantley, S. L. (1992), The effect of fluid chemistry on quartz microcrack lifetimes, *Earth and Planetary Science Letters*, *113*(1-2), 145–156, doi:10.1016/0012-821X(92)90216-I.

Brodsky, E. E., J. D. Kirkpatrick, and T. Candela (2016), Constraints from fault roughness on the scale-dependent strength of rocks, *Geology*, *44*(1), 19–22, doi:10.1130/G37206.1.

Brown, S. R., and C. H. Scholz (1985), Broad bandwidth study of the topography of natural rock surfaces, *Journal of Geophysical Research*, *90*(B14), 12,575, doi:10.1029/JB090iB14p12575.

Candela, T., F. Renard, Y. Klinger, K. Mair, J. Schmittbuhl, and E. E. Brodsky (2012), Roughness of fault surfaces over nine decades of length scales, *Journal of Geophysical Research: Solid Earth*, *117*(B8), n/a–n/a, doi:10.1029/2011JB009041.

Chen, J., and C. J. Spiers (2016), Rate and state frictional and healing behavior of carbonate fault gouge explained using microphysical model, *Journal of Geophysical Research: Solid Earth*, pp. 1–42, doi:10.1002/2016JB013470.

Chester, F. M., and J. S. Chester (1998), Ultracataclasite structure and friction processes of the Punchbowl fault, San Andreas system, California, *Tectonophysics*, *295*(1-2), 199–221, doi:10.1016/S0040-1951(98)00121-8.

Croizé, D., K. Bjørlykke, J. Jahren, and F. Renard (2010), Experimental mechanical and chemical compaction of carbonate sand, *Journal of Geophysical Research*, *115*(B11), B11,204, doi:10.1029/2010JB007697.

De Boer, R. B., P. J. C. Nagtegaal, and E. M. Duyvis (1977), Pressure solution experiments on quartz sand, *Geochimica et Cosmochimica Acta*, *41*(2), 257–264, doi:10.1016/0016-7037(77)90233-2.

De Meer, S., C. J. Spiers, C. J. Peach, and T. Watanabe (2002), Diffusive properties of fluid-filled grain boundaries measured electrically during active pressure solution, *Earth and Planetary Science ...*, *200*, 147–157.

De Meer, S., C. J. Spiers, and S. Nakashima (2005), Structure and diffusive properties of fluid-filled grain boundaries: An in-situ study using infrared (micro) spectroscopy, *Earth and Planetary Science Letters*, *232*(3-4), 403–414, doi:10.1016/j.epsl.2004.12.030.

Desbois, G., J. L. Urai, and J. H. de Bresser (2012), Fluid distribution in grain boundaries of natural fine-grained rock salt deformed at low differential stress (Qom Kuh salt fountain, central Iran): Implications for rheology and transport properties, *Journal of Structural Geology*, *43*, 128–143, doi:10.1016/j.jsg.2012.07.002.

Dewers, T., and A. Hajash (1995), Rate laws for water-assisted compaction and stress-induced water-rock interaction in sandstones, *Journal of Geophysical Research: Solid Earth*, *100*(B7), 13,093–13,112, doi:10.1029/95JB00912.

Dieterich, J. H., and B. D. Kilgore (1996), Imaging surface contacts: power law contact distributions and contact stresses in quartz, calcite, glass and acrylic plastic, *Tectonophysics*, *256*(1-4), 219–239, doi:10.1016/0040-1951(95)00165-4.

Elliott, D. (1973), Diffusion Flow Laws in Metamorphic Rocks, *Geological Society of America Bulletin*, *84*(8), 2645–2664, doi:10.1130/0016-7606(1973)84¡2645:DFLIMR¿2.0.CO;2.

Evans, J. P., and F. M. Chester (1995), Fluid-rock interaction in faults of the San Andreas system: Inferences from San Gabriel fault rock geochemistry and microstructures, *Journal of Geophysical Research*, *100*(B7), 13,007, doi:10.1029/94JB02625.

Ghoussoub, J., and Y. M. Leroy (2001), Solid–fluid phase transformation within grain boundaries during compaction by pressure solution, *Journal of the Mechanics and Physics of Solids*, *49*(10), 2385–2430, doi:http://dx.doi.org/10.1016/S0022-5096(01)00012-6.

Gratier, J., L. Muquet, R. Hassani, and F. Renard (2005), Experimental microstylolites in quartz and modeled application to natural stylolitic structures, *Journal of Structural Geology*, *27*(1), 89–100, doi:10.1016/j.jsg.2004.05.007.

Gratier, J. P. (1987), Pressure solution-deposition creep and associated tectonic differentiation in sedimentary rocks, *Geological Society, London, Special Publications*, *29*(1), 25–38, doi: 10.1144/GSL.SP.1987.029.01.03.

Gratier, J. P., R. Guiguet, F. Renard, L. Jenatton, and D. Bernard (2009), A pressure solution creep law for quartz from indentation experiments, *Journal of Geophysical Research*, *114*(B3), B03,403, doi:10.1029/2008JB005652.

Gratier, J.-p., D. K. Dysthe, and F. Renard (2013), The Role of Pressure Solution Creep in the Ductility of the Earth's Upper Crust, *Advances in Geophysics*, *54*, 47–179, doi:10.1016/B978-0-12-380940-7.00002-0.

Heald, M. T. (1955), Stylolites in sandstones, *The Journal of Geology*, *63*(2), 101–114.

Hickman, S. H., and B. Evans (1991), Experimental pressure solution in halite: the effect of grain/interphase boundary structure, *Journal of the Geological Society*, *148*, 549–560, doi: 10.1144/gsjgs.148.3.0549.

Hickman, S. H., and B. Evans (1992), Growth of Grain Contacts in Halite by Solution-transfer: Implications for Diagenesis, Lithification, and Strength Recovery, in *Fault Mechanics and Transport Properties of Rocks*, edited by B. Evans and T. Wong, pp. 253–280, Academic Press, doi: 10.1016/S0074-6142(08)62825-9.

Holdsworth, R., E. van Diggelen, C. Spiers, J. de Bresser, R. Walker, and L. Bowen (2011), Fault rocks from the SAFOD core samples: Implications for weakening at shallow depths along the San Andreas Fault, California, *Journal of Structural Geology*, *33*(2), 132–144, doi:10.1016/j.jsg.2010.11.010.

Holness, M. B. (1992), Equilibrium dihedral angles in the system quartz-CO2H2ONaCl at 800oC and 1–15 kbar: the effects of pressure and fluid composition on the permeability of quartzites, *Earth and Planetary Science Letters*, *114*(1), 171–184, doi:10.1016/0012-821X(92)90159-S.

Israelachvili, J. N. (1986), *Intermolecular and Surface Forces (With Applications to Colloidal and Biological Systems)*, Academic Press, London.

Jefferies, S., R. Holdsworth, C. Wibberley, T. Shimamoto, C. Spiers, A. Niemeijer, and G. Lloyd (2006), The nature and importance of phyllonite development in crustal-scale fault cores: an example from the Median Tectonic Line, Japan, *Journal of Structural Geology*, *28*(2), 220–235, doi:10.1016/j.jsg.2005.10.008.

Jones, E., T. Oliphant, P. Peterson, and Others (2001), SciPy: Open source scientific tools for Python.

Karner, S. L., C. Marone, and B. Evans (1997), Laboratory study of fault healing and lithification in simulated fault gouge under hydrothermal conditions, *Tectonophysics*, *277*(1-3), 41–55, doi: 10.1016/S0040-1951(97)00077-2.

Karner, S. L., F. M. Chester, A. K. Kronenberg, and J. S. Chester (2003), Subcritical compaction and yielding of granular quartz sand, *Tectonophysics*, *377*(3-4), 357–381, doi:10.1016/j.tecto.2003.10.006.

Lehner, F. K. (1990), Thermodynamics of rock deformation by pressure solution, in *Deformation processes in minerals, ceramics and rocks*, edited by D. J. Barber and P. G. Meredith, pp. 296–333, Unwin Hyman, London.

Lehner, F. K. (1995), A model for intergranular pressure solution in open systems, *Tectonophysics*, *245*(3-4), 153–170, doi:10.1016/0040-1951(94)00232-X.

Lewis, S., and M. Holness (1996), Equilibrium halite-H2O dihedral angles: High rock-salt permeability in the shallow crust?, *Geology*, *24*(5), 431, doi:10.1130/0091-7613(1996)024¡0431:EHHODA¿2.3.CO;2.

Majumdar, A., and C. Tien (1990), Fractal characterization and simulation of rough surfaces, *Wear*, *136*(2), 313–327, doi:10.1016/0043-1648(90)90154-3.

Niemeijer, A. R., and C. J. Spiers (2002), Compaction creep of quartz-muscovite mixtures at 500 C: Preliminary results on the influence of muscovite on pressure solution, *Geological Society, London, Special Publications*, *200*(1), 61–71, doi:10.1144/GSL.SP.2001.200.01.04.

Niemeijer, A. R., and C. J. Spiers (2006), Velocity dependence of strength and healing behaviour in simulated phyllosilicate-bearing fault gouge, *Tectonophysics*, *427*(1-4), 231–253, doi:10.1016/j.tecto.2006.03.048.

Niemeijer, A. R., C. J. Spiers, and B. Bos (2002), Compaction creep of quartz sand at 400-600C: experimental evidence for dissolution-controlled pressure solution, *Earth and Planetary Science Letters*, *195*, 261–275.

Niemeijer, A. R., D. Elsworth, and C. Marone (2009), Significant effect of grain size distribution on compaction rates in granular aggregates, *Earth and Planetary Science Letters*, *284*(3-4), 386–391, doi:10.1016/j.epsl.2009.04.041.

Pluymakers, A. M. H., and C. J. Spiers (2014), Compaction creep of simulated anhydrite fault gouge by pressure solution: theory v. experiments and implications for fault sealing, *Geological Society, London, Special Publications*, *409*(1), 107–124, doi:10.1144/SP409.6.

Raj, R. (1982), Creep in polycrystalline aggregates by matter transport through a liquid phase, *Journal of Geophysical Research*, *87*(B6), 4731, doi:10.1029/JB087iB06p04731.

Renard, F., J. Schmittbuhl, J.-P. Gratier, P. Meaking, and E. Merino (2004), Three-dimensional roughness of stylolites in limestones, *Journal of Geophysical Research*, *109*(B3), B03,209, doi:10.1029/2003JB002555.

Renard, F., S. Beauprêtre, C. Voisin, D. Zigone, T. Candela, D. K. Dysthe, and J. Gratier (2012), Strength evolution of a reactive frictional interface is controlled by the dynamics of contacts and chemical effects, *Earth and Planetary Science Letters*, *344*, 20–34, doi:10.1016/j.epsl.2012.04.048.

Robin, P.-Y. F. (1978), Pressure solution at grain-to-grain contacts, *Geochimica et Cosmochimica Acta*, *42*(9), 1383–1389, doi:10.1016/0016-7037(78)90043-1.

Rutter, E. H. (1976), The kinetics of rock deformation by pressure solution, *Philosophical Transactions of the Royal Society of Londen. Series A, Mathematical and Physical Sciences*, *283*(1312), 203–219.

Rutter, E. H. (1983), Pressure solution in nature, theory and experiment, *Journal of the Geological Society*, *140*(5), 725–740, doi:10.1144/gsjgs.140.5.0725.

Sahimi, M. (2003), *Heterogeneous Materials I: Linear Transport and Optical Properties*, Springer, New York.

Schenk, O., and J. L. Urai (2004), Microstructural evolution and grain boundary structure during static recrystallization in synthetic polycrystals of Sodium Chloride containing saturated brine, *Contributions to Mineralogy and Petrology*, *146*(6), 671–682, doi:10.1007/s00410-003-0522-6.

Schmittbuhl, J., F. Renard, J. P. Gratier, and R. Toussaint (2004), Roughness of Stylolites: Implications of 3D High Resolution Topography Measurements, *Physical Review Letters*, *93*(23), 238,501, doi:10.1103/PhysRevLett.93.238501.

Schutjens, P. M. T. M. (1991), Intergranular pressure solution in halite aggregates and quartz sands: an experimental investigation, Ph.D. thesis, Utrecht University.

Schutjens, P. M. T. M., and C. J. Spiers (1999), Intergranular Pressure Solution in Nacl: Grain-To-Grain Contact Experiments under the Optical Microscope, *Oil & Gas Science and Technology*, *54*(6), 729–750, doi:10.2516/ogst:1999062.

Shanhua, X., R. Songbo, and W. Youde (2015), Three-Dimensional Surface Parameters and Multi-Fractal Spectrum of Corroded Steel, *PLOS ONE*, *10*(6), e0131,361, doi:10.1371/journal.pone.0131361.

Shimizu, I. (1995), Kinetics of pressure solution creep in quartz: theoretical considerations, *Tectonophysics*, *245*(3-4), 121–134, doi:10.1016/0040-1951(94)00230-7.

Sleep, N. H., and M. L. Blanpied (1992), Creep, compaction and the weak rheology of major faults, *Nature*, *359*(6397), 687–692, doi:10.1038/359687a0.

Smeraglia, L., et al. (2017), Microstructural evidence for seismic and aseismic slips along clay-bearing, carbonate faults, *Journal of Geophysical Research: Solid Earth*, doi:10.1002/2017JB014042.

Spiers, C. J., and P. M. T. M. Schutjens (1990), Densification of crystalline aggregates by fluid-phase diffusional creep, in *Deformation processes in minerals, ceramics and rocks*, edited by D. J. Barber and P. G. Meredith, pp. 334–353, Unwin Hyman, London.

Spiers, C. J., P. M. T. M. Schutjens, R. H. Brzesowsky, C. J. Peach, J. L. Liezenberg, and H. J. Zwart (1990), Experimental determination of constitutive parameters governing creep of rocksalt by pressure solution, *Geological Society, London, Special Publications*, *54*(1), 215–227, doi:10.1144/GSL.SP.1990.054.01.21.

Spiers, C. J., S. De Meer, A. R. Niemeijer, and X. Zhang (2004), Kinetics of rock deformation by pressure solution and the role of thin aqueous films, in *Physicochemistry of Water in Geological and Biological Systems*, edited by S. Nakashima, C. J. Spiers, L. Mercury, P. A. Fenter, and M. F. J. Hochella, pp. 129–158, Universal Academy Press, Tokyo.

Stauffer, D., and A. Aharony (1992), *Introduction to Percolation Theory*, 2nd ed., Taylor & Francis, London.

Stöckhert, B., M. Wachmann, M. Küster, and S. Bimmermann (1999), Low effective viscosity during high pressure metamorphism due to dissolution precipitation creep: the record of HP–LT

metamorphic carbonates and siliciclastic rocks from Crete, *Tectonophysics*, *303*(1-4), 299–319, doi:10.1016/S0040-1951(98)00262-5.

Tada, R., and R. Siever (1989), Pressure Solution During Diagenesis, *Annual Review of Earth and Planetary Sciences*, *17*(1), 89–118, doi:10.1146/annurev.ea.17.050189.000513.

Urai, J. L., C. J. Spiers, H. J. Zwart, and G. S. Lister (1986), Weakening of rock salt by water during long-term creep, *Nature*, *324*(6097), 554–557, doi:10.1038/324554a0.

van den Ende, M. P. A., G. Marketos, A. R. Niemeijer, and C. J. Spiers (2018), Investigating Compaction by Intergranular Pressure Solution Using the Discrete Element Method, *Journal of Geophysical Research: Solid Earth*, doi:10.1002/2017JB014440.

Van Noort, R., and C. J. Spiers (2009), Kinetic effects of microscale plasticity at grain boundaries during pressure solution, *Journal of Geophysical Research*, *114*(B3), 1–12, doi:10.1029/2008JB005634.

van Noort, R., C. J. Spiers, and G. M. Pennock (2008), Compaction of granular quartz under hydrothermal conditions: Controlling mechanisms and grain boundary processes, *Journal of Geophysical Research*, *113*(B12), B12,206, doi:10.1029/2008JB005815.

Van Noort, R., H. J. M. Visser, and C. J. Spiers (2008), Influence of grain boundary structure on dissolution controlled pressure solution and retarding effects of grain boundary healing, *Journal of Geophysical Research: Solid Earth*, *113*(3), 1–15, doi:10.1029/2007JB005223.

Visser, H. J. M. (1999), Mass transfer processes in crystalline aggregates containing a fluid phase, Ph.D. thesis, Utrecht University.

Wong, P.-z., J. Howard, and J.-S. Lin (1986), Surface Roughening and the Fractal Nature of Rocks, *Physical Review Letters*, *57*(5), 637–640, doi:10.1103/PhysRevLett.57.637.

Yasuhara, H., C. J. Marone, and D. Elsworth (2005), Fault zone restrengthening and frictional healing: The role of pressure solution, *Journal of Geophysical Research*, *110*, 1–11, doi:10.1029/2004JB003327.

Zahouani, H., R. Vargiolu, and J.-L. Loubet (1998), Fractal models of surface topography and contact mechanics, *Mathematical and Computer Modelling*, *28*(4-8), 517–534, doi:10.1016/S0895-7177(98)00139-3.

Zhang, X., C. J. Spiers, and C. J. Peach (2010), Compaction creep of wet granular calcite by pressure solution at 28C to 150C, *Journal of Geophysical Research*, *115*(B9), B09,217, doi:10.1029/2008JB005853.

Zubtsov, S., F. Renard, J.-P. Gratier, R. Guiguet, D. K. Dysthe, and V. Traskine (2004), Experimental pressure solution compaction of synthetic halite/calcite aggregates, *Tectonophysics*, *385*(1-4), 45–57, doi:10.1016/j.tecto.2004.04.016.